Eur Biophys J (2012) 41:147–159
DOI 10.1007/s00249-011-0766-4

ORIGINAL PAPER

EBSA
Biophysics in Europe

Phases and domains in sphingomyelin–cholesterol membranes: structure and properties using EPR spin-labeling methods

Laxman Mainali · Marija Raguz · Witold K. Subczynski

Received: 11 August 2011 / Revised: 6 October 2011 / Accepted: 11 October 2011 / Published online: 28 October 2011

Abstract EPR spin-labeling methods were used to investigate the order and fluidity of alkyl chains, the hydrophobicity of the membrane interior, and the order and motion of cholesterol molecules in coexisting phases and domains, or in a single phase of fluid-phase cholesterol/egg-sphingomyelin (Chol/ESM) membranes with a Chol/ESM mixing ratio from 0 to 3. A complete set of profiles for these properties was obtained for the liquid-disordered (l_d) phase without cholesterol, for the liquid-ordered (l_o) phase for the entire region of cholesterol solubility in this phase (from 33 to 66 mol%), and for the l_o-phase domain that coexists with the cholesterol bilayer domain (CBD). Alkyl chains in the l_o phase are more ordered than in the l_d pure ESM membrane. However, fluidity in the membrane center is greater. Also, the profile of hydrophobicity changed from a bell to a rectangular shape. These differences are enhanced when the cholesterol content of the l_o phase is increased from 33 to 66 mol%, with clear brake-points between the C9 and C10 positions (approximately where the steroid-ring structure of cholesterol reaches into the membrane). The organization and motion of cholesterol molecules in the CBD are similar to those in the l_o-phase domain that coexists with the CBD.

Keywords Membrane domain · Cholesterol · Liquid-ordered phase · Spin-labeling · EPR · Sphingomyelin

L. Mainali · M. Raguz · W. K. Subczynski (✉)
Department of Biophysics, Medical College of Wisconsin, 8701 Watertown Plank Road, Milwaukee, WI 53226, USA
e-mail: subczyn@mcw.edu

M. Raguz
Department of Medical Physics and Biophysics, School of Medicine, University of Split, Split, Croatia

Introduction

Discrimination and characterization of coexisting membrane phases and domains are not easy tasks. We have developed electron paramagnetic resonance (EPR) spin-labeling methods that provide a unique opportunity to determine the lateral organization of lipid-bilayer membranes by discrimination of coexisting membrane phases and/or domains (Ashikawa et al. 1994; Kawasaki et al. 2001; Raguz et al. 2008, 2009, 2011; Subczynski et al. 2007b; Wisniewska and Subczynski 2008). In some cases, these methods also enable us to characterize coexisting membrane phases and/or domains by using profiles of alkyl-chain order, fluidity, hydrophobicity, and oxygen diffusion-concentration product in situ, without the need for physical separation (Subczynski et al. 2007a, 2010). Here, we will apply these methods to obtain the above-mentioned profiles across lipid-bilayer membranes made of cholesterol (Chol) and egg sphingomyelin (ESM). First, we want to obtain structural and dynamic information about the liquid-ordered (l_o) phase in ESM membranes, because rafts can be regarded as domains of the liquid-ordered phase (Edidin 2003; Ge et al. 1999; London 2002; Simons and Vaz 2004) and/or domains enriched in cholesterol and sphingolipids that compartmentalize cellular processes (Pike 2006). Second, we want to characterize membrane phases and domains formed in these membranes for a wide range of cholesterol content, because sphingolipids and cholesterol are major lipids of human eye lens membranes (Borchman and Yappert 2010; Broekhuyse 1969; Deeley et al. 2008; Li et al. 1987).

Investigations of membranes made from raft-forming ternary lipid mixtures containing sphingomyelin as a saturated phospholipid clearly demonstrate that the l_o phase domain is formed and coexists with the l_d phase domain

(Bunge et al. 2008; Frazier et al. 2007). However, these domains are much smaller than the optical resolution limit and cannot be discriminated by fluorescence microscopy (Veatch and Keller 2003). Estimated sizes vary from 45 to 70 nm (Bunge et al. 2008). These papers also discuss whether cholesterol–phospholipid interactions are better described as l_o and l_d coexisting phases or as condensed complexes of phospholipid and cholesterol (McConnell and Radhakrishnan 2003). EPR spin-labeling methods do not have the limits characteristic of optical methods, and domains containing ~20 lipid molecules can be discriminated and characterized (Ashikawa et al. 1994; Kawasaki et al. 2001; Raguz et al. 2008, 2009, 2011; Subczynski et al. 2007b).

Using lipid spin labels with EPR monitoring groups (free radical nitroxide moieties) located at different depths in the membrane, profiles of different membrane properties across the bilayer can be obtained. Because the molecular structures of these spin labels are similar to those of phospholipids and cholesterol (Fig. S1 in Mainali et al. 2011c), they should, to a some extent, approximate the distribution of phospholipid and cholesterol molecules between membrane domains, and cholesterol–phospholipid and cholesterol–cholesterol interactions in the membrane. For example, phase boundaries for Chol/DMPC (dimyristoylphosphatidylcholine) membranes based on measurements with stearic acid (Kusumi et al. 1986) and phospholipid spin labels (Sankaram and Thompson 1991) overlap with phase boundaries obtained with other methods (Almeida et al. 1992). Similarly, phase boundaries obtained with stearic acid spin labels (Wisniewska and Subczynski 2008) overlap appropriate boundaries in the phase diagram for Chol/palmitoylsphingomyelin (PSM), as presented by de Almeida et al. (2003). Both phospholipid-analogue and cholesterol-analogue spin labels are distributed between the l_o and l_d phases coexisting in Chol/ESM membranes (Fig. 1b in Mainali et al. 2011c), which enables us to discriminate these phases using the discrimination by oxygen transport (DOT) method and to obtain profiles of the oxygen transport parameter (oxygen diffusion–concentration product) across each phase (Mainali et al. 2011c). However, profiles of other properties contain unresolved information from both phases. In ESM membranes with a cholesterol content that exceeds the cholesterol solubility threshold (CST, the CST in ESM membranes is 2; Epand 2003), and when the pure cholesterol bilayer domain (CBD) coexists with the l_o-phase domain, phospholipid-type spin labels should only partition into the bulk l_o-phase domain (Fig. 1f in Mainali et al. 2011c). Thus, in addition to the profile of the oxygen transport parameter, profiles of the order parameter, fluidity, and hydrophobicity can be obtained by use of these spin labels. These profiles should only describe the properties of the bulk l_o-phase domain, without "contamination" from the CBD. Cholesterol analogues, ASL and CSL, should distribute between both domains. Thus, they alone can be used to detect and discriminate the CBD and yield information about this domain (for more detail see Raguz et al. 2008).

The DOT method has been successfully used to discriminate domains in reconstituted membranes crowded with integral membrane proteins (Ashikawa et al. 1994) and in influenza-virus envelope membranes, which contain cholesterol-rich and protein-rich raft domains (Kawasaki et al. 2001). In model membranes made from a binary mixture of phospholipids and cholesterol, l_o, l_d, and solid-ordered phases were distinguished and characterized in different regions of a phase diagram when they formed a single phase or when two phases coexisted (Mainali et al. 2011c; Subczynski et al. 2007b; Wisniewska and Subczynski 2008). In membranes made from a ternary raft-forming mixture, the raft domain was also distinguished from bulk lipids using the DOT method (Wisniewska and Subczynski 2006a, b). In recent studies, we applied the DOT method to discriminate the l_d and l_o phases and the CBD formed in ESM membranes at different cholesterol content (Mainali et al. 2011c).

The main focus of this paper is to complete our previous studies (Mainali et al. 2011c) by providing detailed profiles of the order parameter, fluidity, and hydrophobicity across phases and domains in Chol/ESM membranes. More broadly, we want to compare results obtained for membranes made of lens lipid membranes with those obtained for simple, two-component membranes (made of commercially available lipids) that reflect the basic lipid composition of lens membranes. This comparison gives us an opportunity to better elucidate the major factors that determine specific membrane properties. We have previously investigated POPC-cholesterol membranes (Subczynski et al. 2003; Widomska et al. 2007a) because PC is the major phospholipid in the eye-lens membranes of short-lifespan animals (in mice, PC accounts for ~46% of the total phospholipid composition whereas SM accounts for 15% Deeley et al. 2008). The opposite is true for human eyes, where sphingomyelins account for 66% of the total phospholipid composition and PC accounts for only 11% (Borchman et al. 2004; Deeley et al. 2008). Although human eye-lens membranes contain ~19% SM and ~47% DHSM (dihydrosphingomyelin), we made model measurements using only ESM. There are two reasons for this decision. First, commercially available ESM is a natural phospholipid that contains ~86% palmitoyl SM, and, in humans, palmitate is the most abundant alkyl chain in both SM (~40%) and DHSM (~55%) (Deeley et al. 2008; Yappert et al. 2003). Second, commercially available DHSM contains only a six-carbon chain, which makes this phospholipid irrelevant biologically (Avanti Polar Lipids, Alabaster, AL,

USA). We performed measurements at the same Chol/ESM mixing ratios ((a) 0, (b) 1:4, (c) 1:2, (d) 1:1, (e) 2:1, and (f) 3:1) as we used previously in Mainali et al. (2011c). The notations (a–f) are the same as those indicated in the phase diagram for Chol/ESM membranes in Fig. 1 in Mainali et al. (2011c). This figure should also be used in this paper as a guideline for presentation and interpretation of the data obtained.

Materials and methods

Materials

Egg sphingomyelin (ESM), cholesterol (Chol), and phospholipid spin labels (1-palmitoyl-2-(*n*-doxylstearoyl)phosphatidylcholine (*n*-PC, where $n = 5$, 7, 10, 12, 14, or 16) and tempocholine-1-palmitoyl-2-oleoylphosphatidic acid ester (T-PC)) were obtained from Avanti Polar Lipids. Nine-doxylstearic acid spin labels (9-SASL), cholestane spin label (CSL), and androstane spin label (ASL) were purchased from Molecular Probes (Eugene, OR, USA). Other chemicals (of at least reagent grade) were purchased from Sigma-Aldrich (St Louis, MO, USA).

Preparation of Chol/ESM membranes

The membranes used in this study are multilamellar dispersions of ESM and cholesterol containing 1 mol% spin label, and were prepared using the film deposition method given in Kusumi et al. (1986) (for more detail see also Mainali et al. (2011c)). Chloroform solutions of ESM, cholesterol, and spin label were mixed to attain the desired mixing ratio. Chloroform was evaporated with a stream of nitrogen and with the test tube in constant rotation in order to deposit a uniform film of lipid over the bottom of the tube. The lipid film was thoroughly dried under reduced pressure (0.1 mm Hg) for 12 h. A buffer solution (0.2 mL 10 mM PIPES and 150 mM NaCl, pH 7.0) was added to and vigorously mixed with the dried lipids at 50°C. The buffer used for samples with 9-SASL was 0.1 M borate at pH 9.5. A rather high pH was chosen in this case to ensure that all 9-SASL carboxyl groups were ionized in the ESM membranes (Kusumi et al. 1982a). The properties of ESM membranes should be insensitive to pH in the range 5–11 because ionization of the polar phosphatidylcholine headgroups does not change in this range (Papahadjopoulos 1968).

EPR measurements

The membranes were centrifuged briefly, and the loose pellet was used for EPR measurements. The sample was placed in a 0.6 mm i.d. capillary made of gas-permeable methylpentene polymer, called TPX (Hyde and Subczynski 1989). Samples were thoroughly deoxygenated, yielding correct EPR line shapes and values of the spin–lattice relaxation time.

Conventional EPR spectra were obtained at 40°C with a Bruker EMX spectrometer with temperature-control accessories. A temperature of 40°C was chosen to ensure that measurements were done above the phase transition temperature of ESM membranes (de Almeida et al. 2003; Quinn and Wolf 2009; Wisniewska and Subczynski 2008). EPR spectra were recorded with a modulation amplitude of 1.0 G and an incident microwave power of 5.0 mW. $A'_{\|}$ and $A'_{\perp}$ values were measured directly from the EPR spectra as indicated in Fig. 1. The order parameter was calculated as described in detail by Marsh (1981). Because of the sharpness of the EPR lines and the method of measurements, $A'_{\|}$ and $A'_{\perp}$ values could be measured with an accuracy of ±0.1 G, and the order parameter could be evaluated with an accuracy of ±0.015. Also, maximum splitting values could be measured with an accuracy of ±0.1 G, and the mobility parameter h_+/h_0 values with an accuracy of ±5%. To measure hydrophobicity, the *z*-component of the hyperfine interaction tensor of the *n*-PC or 9-SASL, A_Z, was determined from the EPR spectra for samples frozen at −165°C and recorded with a modulation amplitude of 2.0 G and an incident microwave power of 2.0 mW (Subczynski et al. 1994). $2A_Z$ values were measured with an accuracy of ±0.25 G.

The T_1s of the spin labels were determined by analyzing the saturation-recovery (SR) signal of the central line obtained by short-pulse SR EPR at the X-band (Subczynski et al. 1989; Yin and Subczynski 1996) and used to draw fluidity profiles across membranes. The SR spectrometer used in these studies has been described elsewhere (Yin and Subczynski 1996). A relatively low level of observing power (8 μW, with a loop-gap resonator delivering an H_1 field of 3.6×10^{-5} gauss) was used for all experiments to avoid microwave power saturation (which induces artificial shortening of the apparent T_1). Accumulations of the decay signals were carried out with 2,048 data points on each decay. SR signals were fitted by use of single-exponential or double-exponential functions. When a single-exponential fit was satisfactory, the uncertainties in the measurements of decay time from the fits were usually less than 0.05%, whereas the decay times determined from sample to sample (for samples prepared totally independently) were within an accuracy of ±3%. When a double-exponential fit was necessary, and satisfactory, the decay times were usually evaluated with standard deviations less than ±5 and ±10% for longer and shorter recovery time constants, respectively. Larger standard deviations for shorter components are because of the difficulty of measuring very

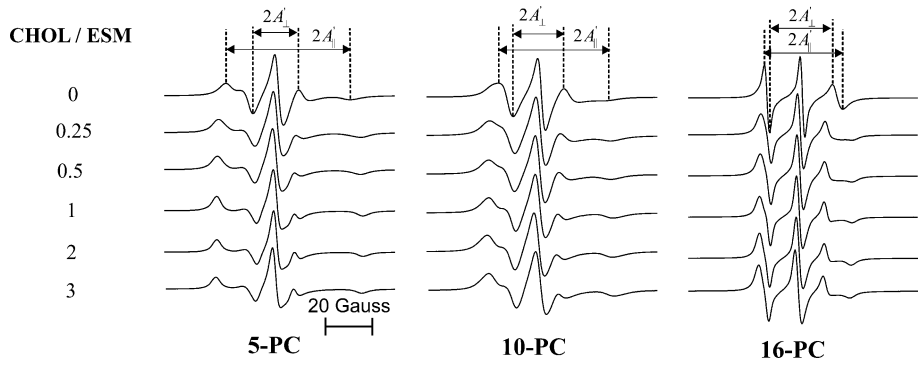

Fig. 1 EPR spectra of 5, 10, and 16-PC in membranes made of Chol/ESM mixtures with Chol/ESM mixing ratios from 0 to 3. Spectra were recorded at 40°C. Measured values for evaluating the order parameter are indicated. The positions of specific peaks were evaluated with high accuracy by monitoring them at 10 times higher receiver gain and, when necessary, a higher modulation amplitude

short T_1s (because of the presence of molecular oxygen) in the current setting of the instrument. It is also possible that the available pump power cannot saturate the signal when the T_1 is very short.

Results and discussion

Order and fluidity of alkyl chains

Conventional EPR spectra were recorded for each spin label and for all cholesterol content of the ESM membranes indicated in the "Introduction" and in the phase diagram in Mainali et al. (2011c). Remarkably, these spectra contained no clearly visible conventional features indicating the presence of two components. This is consistent with our earlier conventional EPR studies of PC/cholesterol membranes (Subczynski et al. 2007b), suggesting that, without special analysis, the features of two coexisting domains cannot be evaluated separately. In this work, the problem of unresolved EPR spectra for n-PC and n-SASL exists only for one cholesterol content in the ESM membrane—for membranes made with a Chol/ESM mixing ratio of 1/4. At this cholesterol content, the l_o phase coexists with the l_d phase (Fig. 1b of Mainali et al. 2011c), and spin labels are distributed between these domains. However, when the l_o-phase domain coexists with the CBD, the EPR spectra from phospholipid-type spin labels located in the l_o-phase domain are not "contaminated" from the pure CBD (see the "Introduction" for more explanation).

Figure 1 shows a set of conventional EPR spectra obtained from 5, 10, and 16-PC in ESM membranes with different cholesterol content. Figure 2 shows profiles of the order parameter obtained across ESM membranes with different cholesterol content. All profiles have an inverted-bell shape and show that alkyl-chain order gradually decreases with depth in the membrane. Values of the order parameter measured at the same depth are always significantly greater for ESM membranes containing cholesterol than for those measured for pure ESM membranes. Thus, the ordering effect of cholesterol is observed at all depths from the membrane surface to the membrane center. At a Chol/ESM mixing ratio of 1/4, the order parameter already increases significantly at all depths. According to the phase diagram shown in Fig. 1 of Mainali et al. (2011c), at 40°C variations in the overall cholesterol content between $\sim$7.5 and $\sim$30 mol% affect fractions of the l_d and l_o phases (each phase contains a constant concentration of 7.5 and 30 mol% cholesterol, respectively). Thus, at a Chol/ESM mixing ratio of 1/4, approximately 51% of ESM molecules is in the l_d-phase, and 49% is in the l_o-phase. Knowledge of the partitioning of phospholipid spin labels into both phases would enable us to evaluate the contribution of EPR signals from the l_o and l_d phases. Although we were unable to evaluate these partition coefficients, even without this knowledge we were able to draw correct profiles for the oxygen transport parameter across coexisting domains (Mainali et al. 2011c). Chiang et al. (2005) and Swamy et al. (2006) successfully carried out a nonlinear least-squares analysis of conventional EPR spectra, found coexisting l_o and l_d phases in model membranes made from ternary lipid mixtures, and evaluated partition coefficients for 5, 7, 10, 12, 14, and 16-PC between these phases. These coefficients increase with an increase in the depth of the location of the nitroxide moiety in membranes from 0.4 to 1.1. Partition coefficients were found to differ for the different compositions of coexisting phases (Chiang et al. 2005). In a binary mixture of dipalmitoyl-PC and cholesterol, the partition coefficient of 16-PC was shown to be slightly greater than unity, indicating that 16-PC favors the l_o phase slightly over the l_d phase (Chiang et al. 2007).

A major increase in the order parameter occurs when the l_o phase already occupies the entire membrane (at a Chol/ESM mixing ratio of 1/2). We were able to show that further addition of cholesterol causes a shift of order-parameter profiles to higher values, indicating increased ordering of the l_o phase when the cholesterol content in this

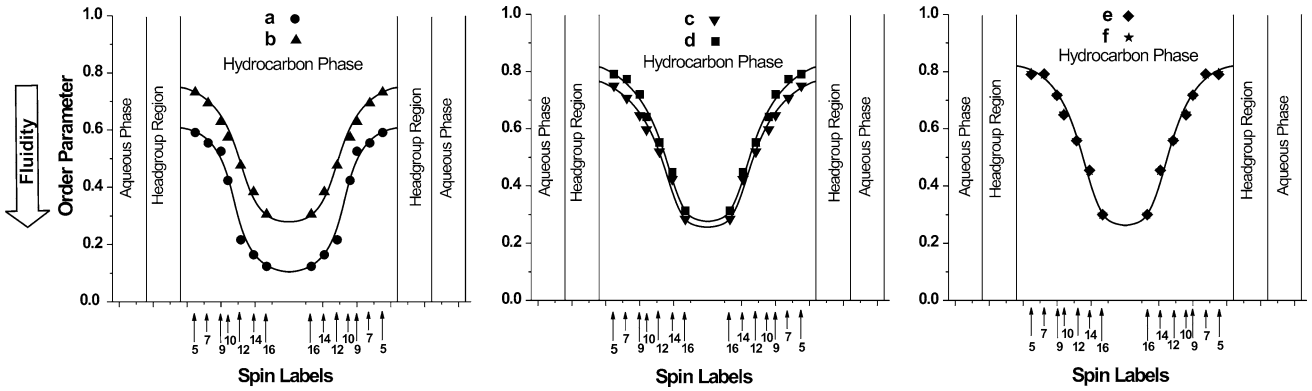

Fig. 2 Profiles of the order parameter across Chol/ESM membranes obtained at Chol/ESM mixing ratios of **a** 0, **b** 1:4, **c** 1:2, **d** 1:1, **e** 2:1, and **f** 3:1 (schemes for membrane structures are shown in Fig. 1 of Mainali et al. 2011c). Approximate locations of nitroxide moieties of spin labels are indicated by *arrows*

phase increases from the minimum value (at a Chol/ESM molar ratio of $\sim 1/2$) to the maximum value (at the CST). These changes are pronounced close to the membrane surface and negligible at the membrane center. Our order parameter data are in agreement with data obtained for PSM and Chol/PSM membranes using solid-state ^{2}H NMR spectroscopy (Bartels et al. 2008). At a Chol/ESM mixing ratio higher than 2/1 (higher than the CST), the l_o-phase domain contains 66 mol% cholesterol; the excess of cholesterol will form the immiscible pure CBD. EPR spectra (Fig. 1) and order parameter profiles (Fig. 2e, f) show that the presence of the CBD does not change the order parameter in the l_o-phase domain.

Profiles of the order parameter, which are routinely used as a measure of membrane fluidity, describe static membrane properties—namely, amplitudes of the wobbling motion of alkyl chains. Therefore, we have also used T_1 here as a convenient quantitative measure of the rate of alkyl-chain motion of n-PC and n-SASL in the ESM lipid bilayer. This parameter depends primarily on the rate of motion of the nitroxide moiety within the lipid bilayer and describes the dynamics of the membrane environment at the depth at which the nitroxide fragment is located. Thus, T_1 can be used as a convenient quantitative measure of membrane fluidity that reports on the rate of motion of phospholipid alkyl chains (or nitroxide free-radical moieties attached to those chains; Mainali et al. 2011a). Smaller T_1 values indicate a greater rate of motion and higher membrane fluidity. Figure 3 shows representative SR signals of 5-PC in ESM membranes for different cholesterol content. SR measurements were carried out systematically as a function of the location of spin labels in the membrane (showing that all SR signals can be satisfactorily fit to single-exponential functions). All SR measurements were performed for deoxygenated samples.

Fluidity profiles (T_1 vs. depth in the membrane) are presented in Fig. 4. As expected, membrane fluidity (membrane dynamics) increases toward the center of all membranes (which is indicated by a decrease in T_1). As shown by comparing profiles for the pure ESM membrane and ESM membranes containing cholesterol, cholesterol reduces membrane fluidity close to the membrane surface (5 and 7-PC positions) and increases it in the membrane center (14 and 16-PC positions). The breaking point between the rigidifying and fluidizing effects of cholesterol lies around the C9 and C10 positions, the depth at which the ring-structure of cholesterol is immersed into the bilayer. The order parameter (which describes a static membrane property) cannot differentiate the effects of cholesterol at different depths, whereas the oxygen transport parameter—a dynamic parameter—clearly shows differences between the membrane region where the cholesterol ring-structure is located and the dipper region where the isooctyl chain of cholesterol is located (Subczynski et al. 1989). These results reveal new characteristics of the l_o phase compared with the l_d phase without cholesterol, indicating that the dynamics of alkyl chains are slightly suppressed close to the membrane surface when the l_o phase is formed (T_1 of 5-PC increases by $\sim 3\%$) and significantly increased in the membrane center (T_1 of 16-PC decreases by $\sim 25\%$). Further addition of cholesterol enhances the differences between the l_o phase and the pure ESM membrane. Also, it shows that the l_o phase saturated with cholesterol (Chol/ESM mixing ratio of 2/1) becomes less fluid close to the membrane surface and more fluid in the membrane center than the l_o phase with a minimum cholesterol concentration (Chol/ESM mixing ratio of 1/2).

Hydrophobicity of membrane interior

Hydrophobicity profiles were constructed by plotting $2A_Z$ values as a function of the position of the nitroxide moiety across the ESM membrane (Subczynski et al. 1994). Figure 5 contains representative EPR spectra of 14-PC in a

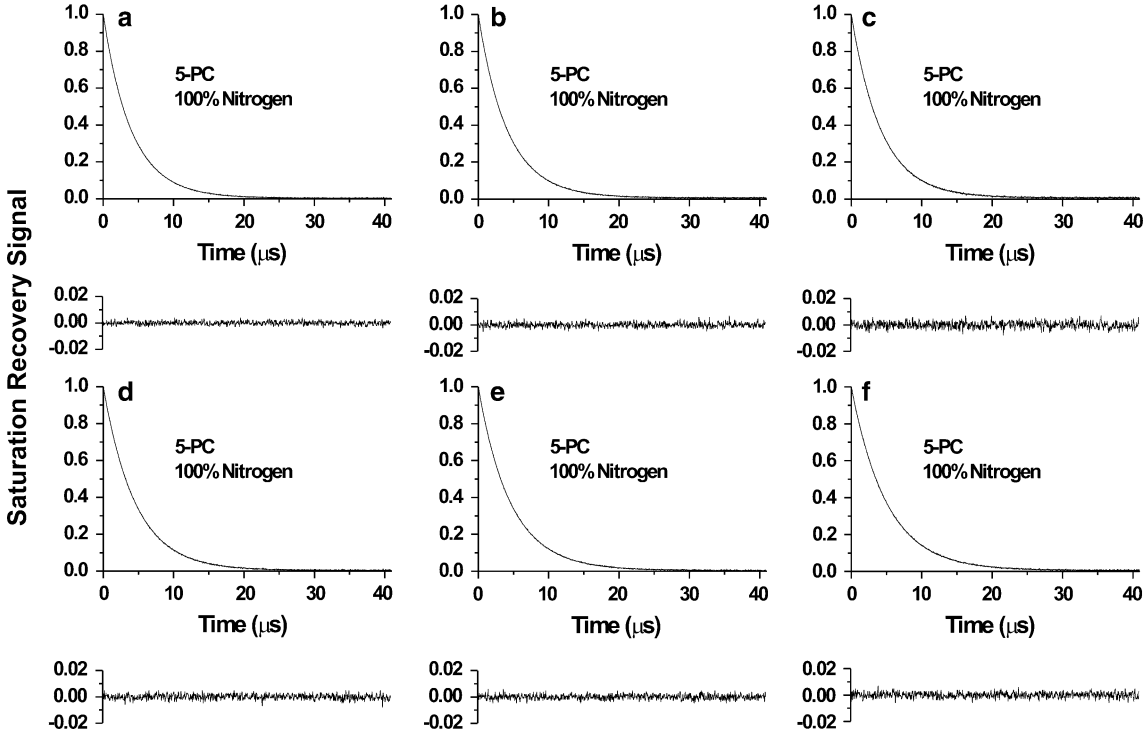

Fig. 3 Representative SR signals with fitted curves and the residuals (the experimental signal minus the fitted curve) for 5-PC spin label in Chol/ESM membranes obtained at Chol/ESM mixing ratios of **a** 0, **b** 1:4, **c** 1:2, **d** 1:1, **e** 2:1, and **f** 3:1 (schemes for membrane structures are shown in Fig. 1 of Mainali et al. 2011c). Membrane specimens were equilibrated with nitrogen. SR signals were satisfactorily fitted to a single exponential function with time constants of **a** 4.10 ± 0.01 μs, **b** 4.17 ± 0.01 μs, **c** 4.22 ± 0.01 μs, **d** 4.60 ± 0.01 μs, **e** 4.70 ± 0.01 μs, and **f** 4.95 ± 0.01 μs

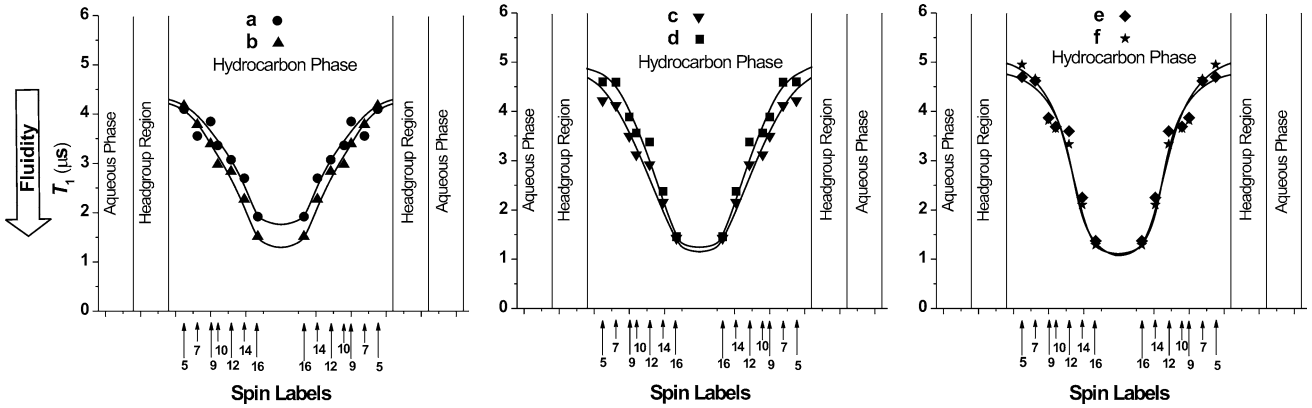

Fig. 4 Profiles of the electron spin–lattice relaxation time, T_1, (fluidity profiles) for n-PC spin labels across Chol/ESM membranes obtained at Chol/ESM mixing ratios of **a** 0, **b** 1:4, **c** 1:2, **d** 1:1, **e** 2:1, and **f** 3:1 (schemes for membrane structures are shown in Fig. 1 of Mainali et al. 2011c). Approximate locations of the nitroxide moieties of spin labels are indicated by *arrows*

frozen solution of ESM membranes and shows the method of measuring $2A_Z$ values. Smaller $2A_Z$ values indicate higher hydrophobicity. Thus, changes in spectra of 14-PC (Fig. 5) indicate that the membrane interior becomes more hydrophobic in the presence of cholesterol. For brevity, we relate the local hydrophobicity as observed by $2A_Z$ to the hydrophobicity (or ε) of the bulk organic solvent by referring to Fig. 2 in Subczynski et al. (1994).

Figure 6 shows hydrophobicity profiles obtained across ESM membranes for different cholesterol content. All profiles contain information from a single phase or a single domain except for the profile obtained at a Chol/ESM mixing ratio of 1/4, when the l_o phase coexists with the l_d phase (Fig. 1b of Mainali et al. 2011c; explained in the section "Order and fluidity of alkyl chains"). Because measurements of membrane hydrophobicity are performed

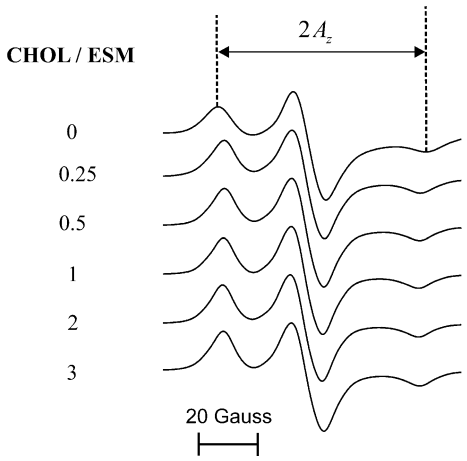

Fig. 5 EPR spectra of 14-PC in membranes made of Chol/ESM mixtures with Chol/ESM mixing ratios from 0 to 3. Spectra were recorded at −165°C. The measured $2A_Z$ value (z-component of the hyperfine interaction tensor) is indicated

for frozen samples, measured $2A_Z$ values indicate the averaged hydrophobicity of the l_o and l_d-phase domains. Nevertheless, hydrophobicity in the hydrocarbon region of the membrane at this cholesterol content is significantly higher than that in the pure ESM membrane, but not as high as that in the l_o-phase domain containing the smallest concentration of cholesterol (~30 mol%). However, in the polar headgroup region, hydrophobicity (measured with T-PC) decreases significantly. This is understandable, because the presence of cholesterol separates polar headgroups and extends water penetration into that region (Subczynski et al. 1994).

The effects of cholesterol can be summarized as follows. The profile for the pure ESM membrane is practically flat, with membrane hydrophobicity comparable with that of ethanol ($\varepsilon = \sim 30$; although it is still considerably less polar than in the bulk aqueous phase ($\varepsilon = 80$)). After the first addition of cholesterol, the profile becomes trapezoidal in shape. Membrane hydrophobicity gradually increases from the membrane surface to the depth of C10, increasing from a value comparable with that of ethanol ($\varepsilon = \sim 30$) to that of hexane ($\varepsilon = \sim 2$), and stays constant at deeper locations. Further addition of cholesterol, up to the CST, increases the sharpness of the change in hydrophobicity. The profile becomes rectangular, with low hydrophobicity up to the depth of C9 and high hydrophobicity in the membrane center. An abrupt change in hydrophobicity occurs between C9 and C10. The profile becomes typical for membranes saturated with cholesterol. In the polar headgroup region, addition of cholesterol causes an increase in polarity which stabilizes after formation of the l_o phase in the entire membrane.

Order and motion of cholesterol molecules (with special attention paid to the CBD)

Figure 7 shows conventional EPR spectra for cholesterol-analogue spin labels ASL and CSL in Chol/ESM membranes with a mixing ratio from 0 to 3. The CST in the ESM membranes is 2 (Epand 2003). Thus, with a Chol/ESM mixing ratio of 3, approximately 66% of cholesterol molecules should saturate the ESM bilayer and 33% should form the CBD. With this assumption, we can obtain EPR spectra of ASL and CSL from the CBD by subtracting the signal obtained for the Chol/ESM mixing ratio of 2 (with a weight of 0.66) from that obtained for the Chol/ESM mixing ratio of 3. These spectra are included in Fig. 7 and are indicated as "CBD". This procedure is valid only when the distribution of cholesterol analogue spin labels between the CBD and the surrounding ESM membrane saturated with cholesterol is close to the distribution of cholesterol. In our previous paper (Raguz et al. 2011), we confirmed this assumption. Pre-exponential factors, obtained for

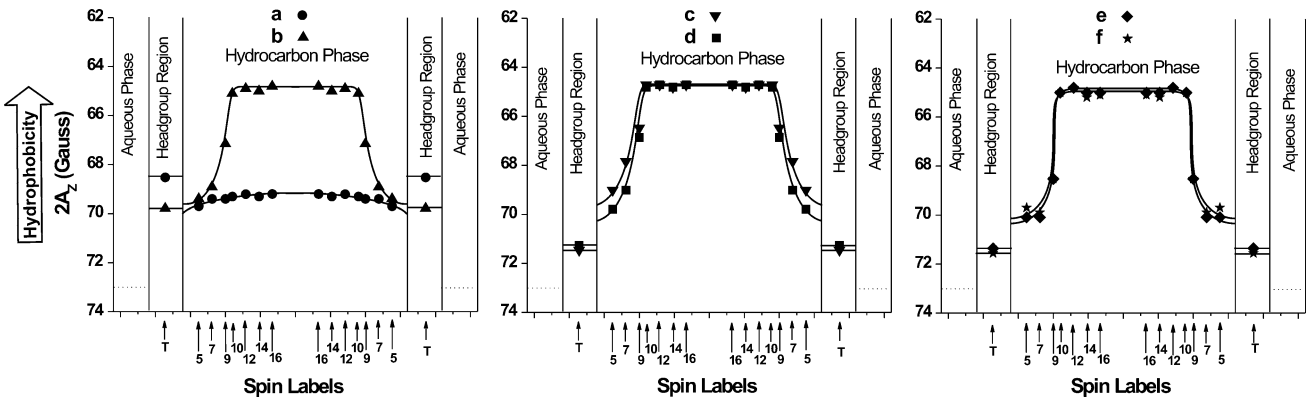

Fig. 6 Hydrophobicity profiles ($2A_Z$) across Chol/ESM membranes obtained at Chol/ESM mixing ratios of **a** 0, **b** 1:4, **c** 1:2, **d** 1:1, **e** 2:1, and **f** 3:1 (schemes for membrane structures are shown in Fig. 1 of Mainali et al. 2011c). Upward changes indicate increases in hydrophobicity. *Dotted lines* indicate hydrophobicity in the aqueous phase. Approximate locations of nitroxide moieties of the spin labels are indicated by *arrows*

double-exponential saturation-recovery curves in the presence of relaxation agents (oxygen for ASL and NiEDDA for CSL), indicate populations of ASL and CSL in the CBD and the surrounding membrane. We showed that the ratio of these populations was very close to the calculated distribution of cholesterol molecules between the CBD and the surrounding membrane saturated with cholesterol.

EPR spectra presented in Fig. 7 have three features:

1. there is no clear indication of the presence of two components, even at the highest cholesterol content;
2. all spectra are characteristic of spin labels in lipid-bilayer-like structures; and
3. changes in the overall shape of the spectra that occur after addition of cholesterol to the ESM membrane up to the CST indicate a significant increase in molecular order and a decrease in the fluidity of the lipid bilayer.

Further addition of cholesterol (above the CST) hardly affects the overall shape of the spectra. Changes in the spectra were evaluated by use of the sets of parameters indicated in Fig. 7 and plotted as a function of cholesterol content in Fig. 8. These parameters are, maximum splitting

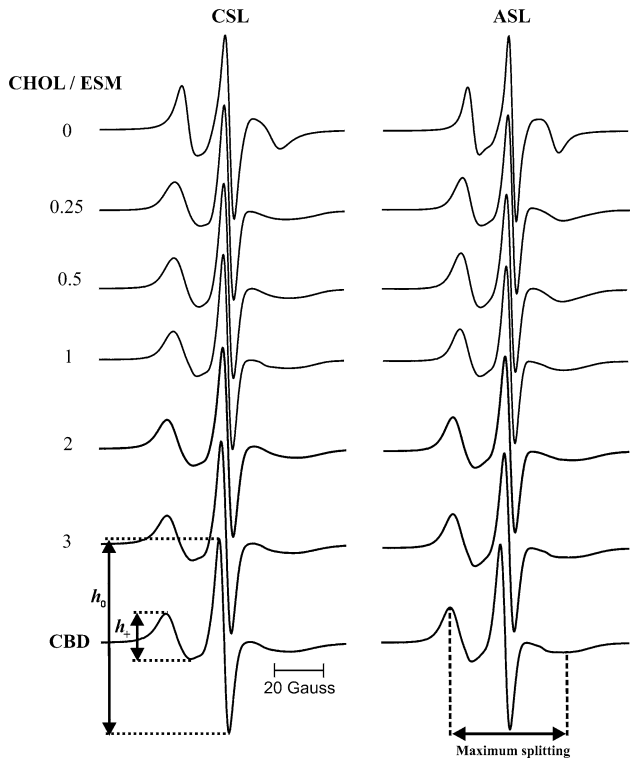

Fig. 7 EPR spectra of CSL and ASL in membranes made of Chol/ESM mixtures with Chol/ESM mixing ratios from 0 to 3. Spectra were recorded at 40°C. "CBD" indicates EPR spectra of CSL and ASL located in the CBD (see the section "Order and motion of cholesterol molecules (with special attention paid to the CBD)" and Raguz et al. 2011 for details of the subtraction procedure). Measured values, maximum splitting, h_+, h_0, are indicated

(Fig. 8a, a parameter related to the order parameter, which indicates the amplitude of the wobbling motion of the long axes of the ASL and CSL molecules; Kusumi et al. 1986) and the h_+/h_0 ratio (Fig. 8b, a parameter that includes contribution of both the orientation and rotational mobility of the ASL and CSL molecules; Schreier et al. 1978). Differences between the maximum-splitting values of the EPR spectra of ASL and CSL in the CBD and in the l_o-phase domain saturated with cholesterol are negligible (Fig. 8a). Similarly, the spectral parameter h_+/h_0, which describes the order and dynamics of both the ASL and CSL molecules, is the same in the CBD and in the l_o-phase domain saturated with cholesterol (Fig. 8b).

Here, we also used T_1 as a convenient quantitative measure of the rate of motion of ASL and CSL in the ESM membrane. Figure 8c shows T_1 values for ASL and CSL in ESM membranes as a function of cholesterol content. As we have shown previously (Mainali et al. 2011c), there is no indication of two components in the SR signals (measured without relaxation agents), even at the highest cholesterol content, when the coexisting domains, CBD, and the l_o-phase domain, are present. Thus, T_1 values in both domains must be very close, indicating a similar rate of motion for cholesterol analogue spin labels. An increase in T_1 values that occurs after the addition of cholesterol to the ESM membrane up to the Chol/ESM mixing ratio of 1 is indicative of reduced motion of cholesterol analogues. After addition of cholesterol up to the Chol/ESM mixing ratio of 2, T_1 values decrease again, practically to their initial values. Further addition of cholesterol (up to the Chol/ESM mixing ratio of 3) does not change T_1 values, indicating that the rate of motion of ASL and CSL should be very similar in the coexisting l_o-phase domain and CBD, which is also in agreement with results presented in Fig. 8b.

Because the nitroxide moiety of ASL and CSL is firmly connected to the rigid sterol-ring structure of cholesterol, its orientation and rotational motion reflect those of the rigid-ring structure of cholesterol. Thus, the above results reveal that cholesterol molecules in the coexisting CBD and l_o-phase domain behave in the same way, with similar order and rate of rotational motion. This is the reason these domains cannot be discriminated by use of conventional EPR spectra of ASL and CSL, or even by SR EPR measurements with these spin labels but without a relaxation agent.

General discussion

The major result that relates to raft research is the characterization of the l_o phase when it is in equilibrium with the l_d phase. Previously, conventional EPR and SR EPR

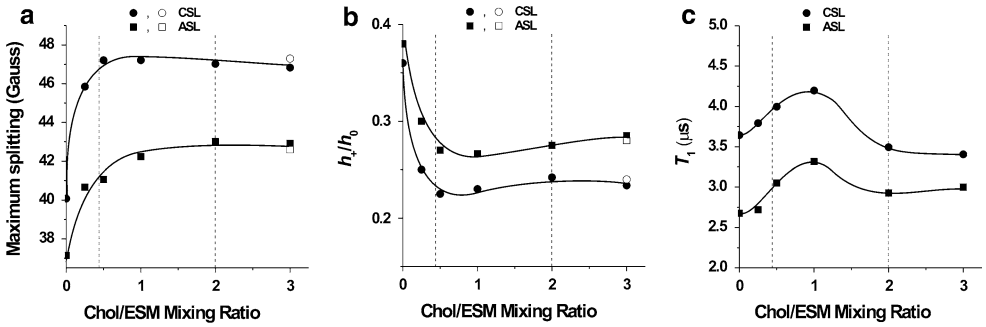

Fig. 8 Spectral parameters, maximum splitting (**a**) and the mobility parameter, h_+/h_0 (**b**), measured for the EPR spectra shown in Fig. 7 are plotted as a function of the Chol/ESM mixing ratio. *Filled symbols* indicate experimental data for ASL and CSL in Chol/ESM membranes, and *open symbols* indicate values obtained for CBD spectra. **c** T_1 values for ASL and CSL measured in deoxygenated samples are plotted as a function of the Chol/ESM mixing ratio. The region of the Chol/ESM mixing ratio in which the single l_o-phase exists is indicated by *broken lines*

were used to indicate coexisting phases in binary mixtures of ESM and cholesterol, providing evidence for the existence of immiscible fluid phases (l_o and l_d) (Wisniewska and Subczynski 2008). More recently, coexisting phases were characterized by use of detailed profiles of the oxygen transport parameter in situ (Mainali et al. 2011c). In this study, in order to gain more insight about the structure and dynamics of ESM membranes in the l_o phase, we obtained profiles of the order parameter and hydrophobicity based on conventional EPR measurements and profiles of membrane fluidity based on SR EPR measurements of the spin–lattice relaxation time of spin labels. Because SR is more sensitive to membrane dynamics on longer time scales than conventional EPR techniques, it is thought to be more suitable for study of the dynamics occurring in the l_o phase. SR EPR spin-labeling methods (particularly the DOT method) cover membrane dynamics in a range 0.1–100 μs whereas conventional EPR methods are sensitive to dynamic processes occurring on a time scale up to ~100 ns. Profiles of membrane properties carry information that is complementary. Profiles of the order parameter (obtained using conventional EPR) provide information about the amplitude of the wobbling motion of the alkyl-chain segment of ESM at a specific depth in the membrane. This is not dynamic information, although these profiles are frequently described as profiles of membrane fluidity. Profiles of T_1 (obtained with SR EPR) are the real profiles of fluidity (dynamics), related to the rate of motion of the alkyl-chain segment of ESM at a specific depth. These two profiles describe the order and dynamics of alkyl chains. Profiles of the oxygen transport parameter can also be obtained by use of SR EPR (Mainali et al. 2011c). Using the DOT method, these profiles can be acquired in coexisting phases and domains, for example the l_o and l_d phases or the l_o phase domain and CBD. These are profiles of membrane fluidity, which report on translational diffusion of molecular oxygen (Subczynski et al. 2010). They provide useful information on the three-dimensional dynamic structure of the liquid-ordered domain because collision rates between molecular oxygen and nitroxide spin labels at specific locations in the membrane are sensitive to the dynamics of *gauche–trans* isomerization of lipid hydrocarbon chains and to the structural nonconformability of neighboring lipids (Kusumi et al. 1982b; Subczynski et al. 1989, 1991). Hydrophobicity of the membrane interior is largely determined by the extent of water penetration, giving rise to a hydrophobicity (polarity) gradient across the bilayer in which the environment becomes increasingly nonpolar as one moves from the membrane surface to the terminus of the lipid alkyl chains (Griffith et al. 1974). Profiles of membrane hydrophobicity are related to the distribution of water molecules across the bilayer, because in the absence of water the hydrocarbon environment of the membrane is highly nonpolar, and it has been shown that dehydration abolishes the hydrophobicity gradient (Griffith et al. 1974).

To better summarize and compare our results, we created Fig. 9, in which we plot specific membrane properties at chosen positions on a profile as a function of cholesterol content. With this approach, we can compare properties in different phases and domains that are formed in ESM membranes at different cholesterol content. We chose four depths in the ESM membrane: close to the membrane surface (C5 position), two depths in the middle of the alkyl chains (C9 and C10 positions), and close to the membrane center (C16 position). The C9 and C10 positions were chosen because the major changes in some profiles occur between these depths. Also, the rigid ring structure of cholesterol is immersed to the depth of C9, and the fluid central region of membranes with cholesterol is located at C10 and deeper.

As shown in Fig. 9a, alkyl-chain order increases rapidly at a Chol/ESM mixing ratio of 1/4 (when the l_o-phase is already formed). Increase in cholesterol content from a

Chol/ESM ratio of 1/2 to the CST causes a small increase in the order parameter close to the membrane surface, but does not change the order parameter in the membrane center. Formation of the CBD does not affect the order in the surrounding l_o-phase domain.

Changes in the rate of alkyl-chain motion (Fig. 9b) are more complex. Formation of the l_o phase, coexisting with the l_d phase, causes a small decrease in the rate of motion at the C5 position, whereas at the C9, C10, and C16 positions the rate of motion of the alkyl chains increases significantly. Addition of cholesterol up to a Chol/ESM mixing ratio of 1/1 causes a significant decrease in the rate of motion at the C5, C9, and C10 positions, which is followed by a gradual decrease on further addition of cholesterol up to a Chol/ESM mixing ratio of 3/1. In the membrane center (C16 position), addition of cholesterol from a Chol/ESM mixing ratio of 1/4–3/1 causes mostly monotonous, but small, increases in the rate of motion. At low cholesterol content, the effect of cholesterol on the rate of motion at the C9 and C10 positions resembles that in the membrane center; at high cholesterol content it resembles that close to the membrane surface. Unresolved SR signals at a Chol/ESM mixing ratio of 1/4 suggest that rates of motion of alkyl chains in the l_o and l_d phases should be very similar. Thus, in the l_d phase saturated with cholesterol (at a cholesterol concentration of ~7.5 mol%) the rate of motion of alkyl chains is greater than in pure ESM membranes at all depths, with the exception of the C5 position where motions are about equal. These new results support our earlier findings about the properties of the l_d phase (Mainali et al. 2011c), where we show that the oxygen transport parameter is greater in the l_d phase saturated with cholesterol than in pure ESM membranes, with the exception of the C5 position where it is approximately equal.

Figure 9d summarizes measurements of the oxygen transport parameter in coexisting and single l_d and l_o phases. An increase in cholesterol concentration in the l_o phase causes a decrease in the oxygen transport parameter at all depths—from the membrane surface to the depth of C9—and an increase in the oxygen transport parameter for locations C10 and deeper. The profile of the oxygen transport parameter across the l_o phase in ESM membranes changes from a bell shape at a low cholesterol concentration of ~30 mol% to a rectangular shape at a maximum cholesterol concentration of 66 mol%. With increased cholesterol concentration, the oxygen transport parameter close to the membrane surface becomes as low as in gel-phase membranes, and in the membrane center it becomes greater than in the center of pure ESM membranes. The

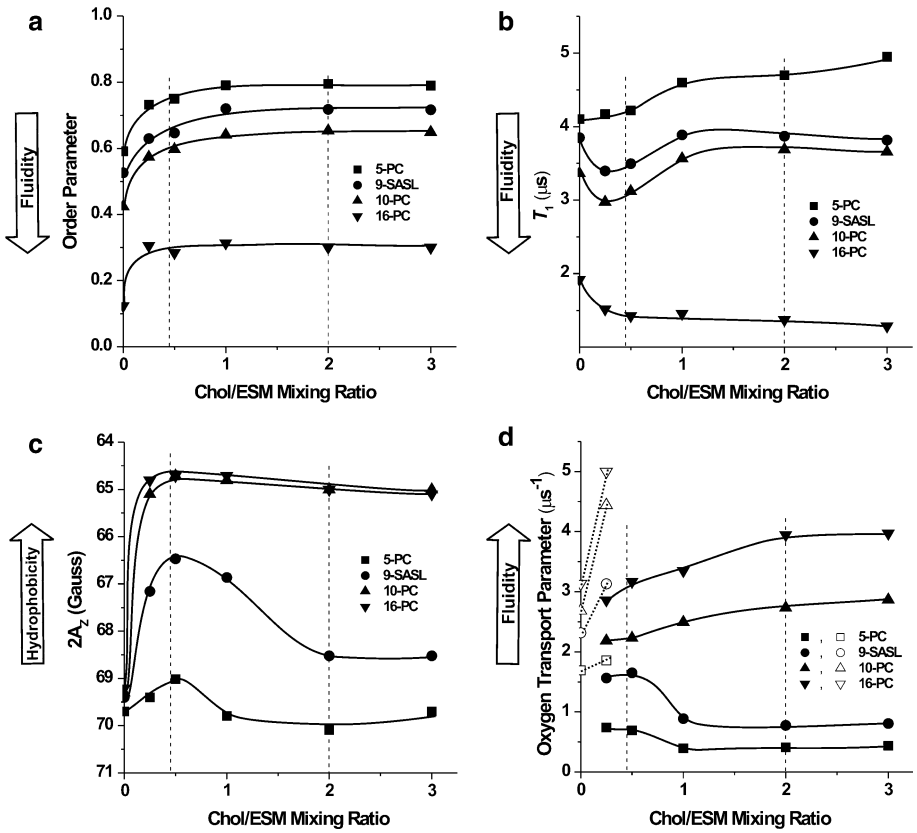

Fig. 9 **a** Order parameter, **b** T_1, **c** hydrophobicity ($2A_Z$), and **d** the oxygen transport parameter obtained at different depth in Chol/ESM membranes are plotted as a function of the Chol/ESM mixing ratio. The region of the Chol/ESM mixing ratio in which the single l_o-phase exists is indicated by *broken lines*

transition from low to high oxygen transport, which is gradual at a low cholesterol concentration, becomes abrupt and occurs within the one C–C bond. Formation of the CBD at cholesterol contents greater than the CST does not affect oxygen transport in the surrounding l_o phase.

Hydrophobicity profiles (Fig. 9c) behave similarly to oxygen transport parameter profiles when cholesterol content increases. After the formation of coexisting l_d and l_o phases, hydrophobicity sharply increases at all depths; it increases further, reaching a maximum, after formation of a single l_o phase which extends to the entire membrane (at a Chol/ESM mixing ratio of 1/2). At higher cholesterol content (only the l_o phase is present) hydrophobicity strongly decreases at depths from the membrane surface to C9 and remains practically unchanged at deeper locations (in the membrane center), which changes the hydrophobicity profile from a bell to a rectangular shape. The change from the polar region to the very hydrophobic region occurs within the one C–C bond (between C9 and C10). These abrupt changes were not observed in the properties of alkyl chains (Figs. 2, 4, 9a, b). However, they are clearly seen when motion and/or distribution of small molecules is measured (Figs. 6, 9c, d). Thus, by using different EPR spin-labeling methods, different membrane properties in the context of membrane depth can be studied and better understood.

Fiber-cell plasma membranes of human lenses are abundant in sphingolipids (Borchman and Yappert 2010; Broekhuyse 1969; Deeley et al. 2008, 2010; Yappert and Borchman 2004; Yappert et al. 2003) and oversaturated with cholesterol (Borchman and Yappert 2010; Deeley et al. 2008; Li et al. 1985, 1987). Interestingly, in lens membranes, a highly saturated sphingolipid content is concomitant with a large amount of cholesterol (Rujoi et al. 2003). Additionally, the CBD should occupy a significant surface of the lipid-bilayer portion of these membranes. Thus, characterization of the l_o-phase domain and the CBD in ESM membranes, when both domains coexist, should contribute to better understanding of the properties of lens-lipid membranes. We would like to emphasize two major findings of this paper.

1. Properties of the l_o-phase domain in the ESM membrane, when it coexists with the CBD (which ensures that the l_o-phase domain is saturated with cholesterol), are very similar to the properties of lens-lipid membranes. The profiles presented across the l_o-phase domain are very similar to those obtained for lens-lipid membranes from 6-month-old bovine (Widomska et al. 2007a, b) and porcine (Raguz et al. 2008) eyes, and from 2-year-old bovine (Raguz et al. 2009) and porcine (Mainali et al. 2011b) eye cortex and nucleus. Our major conclusions from previous publications are confirmed: properties of lens-lipid membranes are determined by the saturating amount of cholesterol and are practically independent of phospholipid composition[1], and the presence of the CBD is significant because it ensures that the surrounding membrane is saturated with cholesterol.
2. We have also confirmed in this study that the CBD is highly dynamic, with motion of cholesterol molecules similar to that in the surrounding ESM membrane saturated with cholesterol. Thus, the exchange rate of cholesterol molecules between the l_o-phase domain and the CBD can be quite high, which suggests that the CBD can be actively involved in the modulation of properties of the lipid-bilayer portion of fiber-cell membranes.

Acknowledgments This work was supported by NIH grants EY015526, TW008052, EB002052, and EB001980.

[1] A reviewer pointed out that our conclusion is in contrast with the commonly accepted statement that membrane saturation reduces membrane fluidity. This difference is clearly seen for lens lipid membranes, where the phospholipid composition changes drastically with age and with a preferential increase in saturated phospholipids, for example sphingomyelin and dihydrosphingomyelin, which should increase the lipid hydrocarbon chain order. Huang et al. (2005) showed that the structural order determined by the static measure of the *trans*/*gauche* rotamer ratio in the hydrocarbon chains increases linearly with the sphingolipid content of the lens lipid membrane (see also the review by Borchman and Yappert 2010). Thus, the properties of lens lipid membranes, including membrane order (fluidity), should change with the age of the donor, between species, and between regions of the lens. However, molecular order, measured with lipid spin labels in saturated membranes, strongly increases with an increase in cholesterol concentration up to ~30 mol%. Further increase of cholesterol concentration, up to 50 mol%, causes a decrease in the molecular order (Kusumi et al. 1986; Sankaram and Thompson 1990; Wisniewska and Subczynski 2008). In unsaturated membranes, the molecular order increases only weakly with an increase in cholesterol concentration up to 50 mol% (Kusumi et al. 1986). Thus, at saturation, both orders are very close. Similar effects were reported by Borchman et al. (1996) using the structural order parameter as a measure of membrane fluidity. The structural order parameter measured in membranes made from bovine nuclear phospholipids (more saturated membranes) increased with cholesterol concentration up to 20–30 mol%, which was then followed by a rapid decrease in the structural order parameter up to ~70 mol% cholesterol. In cortical phospholipid membranes (less saturated membranes), an increase in the structural order parameter induced by cholesterol was significantly weaker. A maximum was reached at ~40 mol% cholesterol. Further increase in cholesterol content also induced a decrease in the structural order parameter. As a result, at cholesterol saturation, the structural order parameters in nuclear and cortical membranes were very close. We should again note that the phospholipid compositions of these two membranes differ substantially. Borchman et al. concluded that the physiological role of cholesterol is to increase the structural order of cortical membrane lipids and reduce the order of nuclear lipids so that the two membranes have a similar order, which is in agreement with our main conclusion.

References

Almeida PFF, Vaz WLC, Thompson TE (1992) Lateral diffusion in the liquid phases of dimyristoylphosphatidylcholine/cholesterol lipid bilayers: a free volume analysis. Biochemistry 31:6739–6747

Ashikawa I, Yin J–J, Subczynski WK, Kouyama T, Hyde JS, Kusumi A (1994) Molecular organization and dynamics in bacteriorhodopsin-rich reconstituted membranes: discrimination of lipid environments by the oxygen transport parameter using a pulse ESR spin-labeling technique. Biochemistry 33:4947–4952

Bartels T, Lankalapalli RS, Bittman R, Beyer K, Brown MF (2008) Raftlike mixtures of sphingomyelin and cholesterol investigated by solid-state 2H NMR spectroscopy. J Am Chem Soc 130:14521–14532

Borchman D, Yappert MC (2010) Lipids and the ocular lens. J Lipid Res 51:2473–2488

Borchman D, Cenedella RJ, Lamba OP (1996) Role of cholesterol in the structural order of lens membrane lipids. Exp Eye Res 62:191–197

Borchman D, Yappert MC, Afzal M (2004) Lens lipids and maximum lifespan. Exp Eye Res 79:761–768

Broekhuyse RM (1969) Phospholipids in tissues of the eye. 3. Composition and metabolism of phospholipids in human lens in relation to age and cataract formation. Biochim Biophys Acta 187:354–365

Bunge A, Muller P, Stockl M, Herrmann A, Huster D (2008) Characterization of the ternary mixture of sphingomyelin, POPC, and cholesterol: support for an inhomogeneous lipid distribution at high temperatures. Biophys J 94:2680–2690

Chiang YW, Zhao J, Wu J, Shimoyama Y, Freed JH, Feigenson GW (2005) New method for determining tie-lines in coexisting membrane phases using spin-label ESR. Biochim Biophys Acta 1668:99–105

Chiang YW, Costa-Filho AJ, Freed JH (2007) Dynamic molecular structure and phase diagram of DPPC-cholesterol binary mixtures: a 2D-ELDOR study. J Phys Chem B 111:11260–11270

de Almeida RF, Fedorov A, Prieto M (2003) Sphingomyelin/phosphatidylcholine/cholesterol phase diagram: boundaries and composition of lipid rafts. Biophys J 85:2406–2416

Deeley JM, Mitchell TW, Wei X, Korth J, Nealon JR, Blanksby SJ, Truscott RJ (2008) Human lens lipids differ markedly from those of commonly used experimental animals. Biochim Biophys Acta 1781:288–298

Deeley JM, Hankin JA, Friedrich MG, Murphy RC, Truscott RJ, Mitchell TW, Blanksby SJ (2010) Sphingolipid distribution changes with age in the human lens. J Lipid Res 51:2753–2760

Edidin M (2003) The state of lipid rafts: from model membranes to cells. Annu Rev Biophys Biomol Struct 32:257–283

Epand RM (2003) Cholesterol in bilayers of sphingomyelin or dihydrosphingomyelin at concentrations found in ocular lens membranes. Biophys J 84:3102–3110

Frazier ML, Wright JR, Pokorny A, Almeida PF (2007) Investigation of domain formation in sphingomyelin/cholesterol/POPC mixtures by fluorescence resonance energy transfer and Monte Carlo simulations. Biophys J 92:2422–2433

Ge M, Field KA, Aneja R, Holowka D, Baird B, Freed JH (1999) Electron spin resonance characterization of liquid ordered phase of detergent-resistant membranes from RBL-2H3 cells. Biophys J 77:925–933

Griffith OH, Dehlinger PJ, Van SP (1974) Shape of the hydrophobic barrier of phospholipid bilayers (evidence for water penetration in biological membranes). J Membr Biol 15:159–192

Huang L, Grami V, Marrero Y, Tang D, Yappert MC, Rasi V, Borchman D (2005) Human lens phospholipid changes with age and cataract. Invest Ophthalmol Vis Sci 46:1682–1689

Hyde JS, Subczynski WK (1989) Spin-label oximetry. In: Berliner LJ, Reuben J (eds) Biological magnetic resonance, vol 8. Plenum Press, New York, pp 399–425

Kawasaki K, Yin J–J, Subczynski WK, Hyde JS, Kusumi A (2001) Pulse EPR detection of lipid exchange between protein rich raft and bulk domains in the membrane: methodology development and its application to studies of influenza viral membrane. Biophys J 80:738–748

Kusumi A, Subczynski WK, Hyde JS (1982a) Effects of pH on ESR spectra of stearic acid spin labels in membranes:probing the membrane surface. Fed Proc 41:1394

Kusumi A, Subczynski WK, Hyde JS (1982b) Oxygen transport parameter in membranes as deduced by saturation recovery measurements of spin-lattice relaxation times of spin labels. Proc Natl Acad Sci USA 79:1854–1858

Kusumi A, Subczynski WK, Pasenkiewicz-Gierula M, Hyde JS, Merkle H (1986) Spin-label studies on phosphatidylcholine-cholesterol membranes: effects of alkyl chain length and unsaturation in the fluid phase. Biochim Biophys Acta 854:307–317

Li LK, So L, Spector A (1985) Membrane cholesterol and phospholipid in consecutive concentric sections of human lenses. J Lipid Res 26:600–609

Li LK, So L, Spector A (1987) Age-dependent changes in the distribution and concentration of human lens cholesterol and phospholipids. Biochim Biophys Acta 917:112–120

London E (2002) Insights into lipid raft structure and formation from experiments in model membranes. Curr Opin Struct Biol 12:480–486

Mainali L, Feix JB, Hyde JS, Subczynski WK (2011a) Membrane fluidity profiles as deduced by saturation-recovery EPR measurements of spin-lattice relaxation times of spin labels. J Magn Reson 212:418–425

Mainali L, Raguz M, Camenisch TG, Hyde JS, Subczynski WK (2011b) Spin-label saturation-recovery EPR at W-band: applications to eye lens lipid membranes. J Magn Reson 212:86–94

Mainali L, Raguz M, Subczynski WK (2011c) Phase-separation and domain-formation in cholesterol-sphingomyelin mixture: pulse EPR oxygen probing. Biophys J 101:837–846

Marsh D (1981) Electron spin resonance: spin labels. Mol Biol Biochem Biophys 31:51–142

McConnell HM, Radhakrishnan A (2003) Condensed complexes of cholesterol and phospholipids. Biochim Biophys Acta 1610:159–173

Papahadjopoulos D (1968) Surface properties of acidic phospholipids: interaction of monolayers and hydrated liquid crystals with uni- and bi-valent metal ions. Biochim Biophys Acta 163:240–254

Pike LJ (2006) Rafts defined: a report on the Keystone symposium on lipid rafts and cell function. J Lipid Res 47:1597–1598

Quinn PJ, Wolf C (2009) Hydrocarbon chains dominate coupling and phase coexistence in bilayers of natural phosphatidylcholines and sphingomyelins. Biochim Biophys Acta 1788:1126–1137

Raguz M, Widomska J, Dillon J, Gaillard ER, Subczynski WK (2008) Characterization of lipid domains in reconstituted porcine lens membranes using EPR spin-labeling approaches. Biochim Biophys Acta 1778:1079–1090

Raguz M, Widomska J, Dillon J, Gaillard ER, Subczynski WK (2009) Physical properties of the lipid bilayer membrane made of cortical and nuclear bovine lens lipids: EPR spin-labeling studies. Biochim Biophys Acta 1788:2380–2388

Raguz M, Mainali L, Widomska J, Subczynski WK (2011) The immiscible cholesterol bilayer domain exists as an integral part of phospholipid bilayer membranes. Biochim Biophys Acta 1808:1072–1080

Rujoi M, Jin J, Borchman D, Tang D, Yappert MC (2003) Isolation and lipid characterization of cholesterol-enriched fractions in

cortical and nuclear human lens fibers. Invest Ophthalmol Vis Sci 44:1634–1642

Sankaram MB, Thompson TE (1990) Interaction of cholesterol with various glycerophospholipids and sphingomyelin. Biochemistry 29:10670–10675

Sankaram MB, Thompson TE (1991) Cholesterol-induced fluid-phase immiscibility in membranes. Proc Natl Acad Sci USA 88:8686–8690

Schreier S, Polnaszek CF, Smith IC (1978) Spin labels in membranes. Problems in practice. Biochim Biophys Acta 515:395–436

Simons K, Vaz WL (2004) Model systems, lipid rafts, and cell membranes. Annu Rev Biophys Biomol Struct 33:269–295

Subczynski WK, Hyde JS, Kusumi A (1989) Oxygen permeability of phosphatidylcholine-cholesterol membranes. Proc Natl Acad Sci USA 86:4474–4478

Subczynski WK, Hyde JS, Kusumi A (1991) Effect of alkyl chain unsaturation and cholesterol intercalation on oxygen transport in membranes: a pulse ESR spin labeling study. Biochemistry 30:8578–8590

Subczynski WK, Wisniewska A, Yin J–J, Hyde JS, Kusumi A (1994) Hydrophobic barriers of lipid bilayer membranes formed by reduction of water penetration by alkyl chain unsaturation and cholesterol. Biochemistry 33:7670–7681

Subczynski WK, Pasenkiewicz-Gierula M, McElhaney RN, Hyde JS, Kusumi A (2003) Molecular dynamics of 1-palmitoyl-2-oleoylphosphatidylcholine membranes containing transmembrane alpha-helical peptides with alternating leucine and alanine residues. Biochemistry 42:3939–3948

Subczynski WK, Widomska J, Wisniewska A, Kusumi A (2007a) Saturation-recovery electron paramagnetic resonance discrimination by oxygen transport (DOT) method for characterizing membrane domains methods in molecular biology, lipid rafts, vol 398. Humana Press, Totowa, pp 143–157

Subczynski WK, Wisniewska A, Hyde JS, Kusumi A (2007b) Three-dimensional dynamic structure of the liquid-ordered domain in lipid membranes as examined by pulse-EPR oxygen probing. Biophys J 92:1573–1584

Subczynski WK, Raguz M, Widomska J (2010) Studying lipid organization in biological membranes using liposomes and EPR spin labeling. Methods Mol Biol 606:247–269

Swamy MJ, Ciani L, Ge M, Smith AK, Holowka D, Baird B, Freed JH (2006) Coexisting domains in the plasma membranes of live cells characterized by spin-label ESR spectroscopy. Biophys J 90:4452–4465

Veatch SL, Keller SL (2003) Separation of liquid phases in giant vesicles of ternary mixtures of phospholipids and cholesterol. Biophys J 85:3074–3083

Widomska J, Raguz M, Dillon J, Gaillard ER, Subczynski WK (2007a) Physical properties of the lipid bilayer membrane made of calf lens lipids: EPR spin labeling studies. Biochim Biophys Acta 1768:1454–1465

Widomska J, Raguz M, Subczynski WK (2007b) Oxygen permeability of the lipid bilayer membrane made of calf lens lipids. Biochim Biophys Acta 1768:2635–2645

Wisniewska A, Subczynski WK (2006a) Accumulation of macular xanthophylls in unsaturated membrane domains. Free Radic Biol Med 40:1820–1826

Wisniewska A, Subczynski WK (2006b) Distribution of macular xanthophylls between domains in a model of photoreceptor outer segment membranes. Free Radic Biol Med 41:1257–1265

Wisniewska A, Subczynski WK (2008) The liquid-ordered phase in sphingomyelin-cholesterol membranes as detected by the discrimination by oxygen transport (DOT) method. Cell Mol Biol Lett 13:430–451

Yappert MC, Borchman D (2004) Sphingolipids in human lens membranes: an update on their composition and possible biological implications. Chem Phys Lipids 129:1–20

Yappert MC, Rujoi M, Borchman D, Vorobyov I, Estrada R (2003) Glycero- versus sphingo-phospholipids: correlations with human and non-human mammalian lens growth. Exp Eye Res 76:725–734

Yin J-J, Subczynski WK (1996) Effects of lutein and cholesterol on alkyl chain bending in lipid bilayers: a pulse electron spin resonance spin labeling study. Biophys J 71:832–839